Antenna Array Beamforming for Low Probability of Intercept Radars

by

Daniel Goad

A thesis submitted to the Graduate Faculty of
Auburn University
in partial fulfillment of the
requirements for the Degree of
Master of Science

Auburn, Alabama
December 14, 2013

Keywords: Radar, Low Probability of Intercept, LPI, Antenna Arrays, Beamforming

Approved by

Lloyd Riggs, Chair, Professor of Electrical and Computer Engineering
Michael Baginski, Associate Professor of Electrical and Computer Engineering
Shumin Wang, Associate Professor of Electrical and Computer Engineering
Stuart Wentworth, Associate Professor of Electrical and Computer Engineering

Abstract

A radar system's focus on low probability of intercept (LPI) performance has become increasingly important as systems designed for electronic support measures (ESM) and electronic counter measures (ECM) continue to become more prevalent. Due to the inherent two-way versus one-way propagation loss of a transmitted signal, radar systems are often highly visible to intercept receivers, and thus have a high probability of detection. A novel transmit array beamforming approach has been introduced that offers significant LPI performance gains for radar systems using a one-dimensional phased antenna array. This method replaces the traditional high-gain scanned beam with a set of low-gain, spoiled beams scanned across the same observation area. A weighted summation of these spoiled beams can result in a return equivalent to that of the traditional high-gain pattern. As a result, the antenna performance of the radar system remains unchanged while the peak gain of the transmitted signal is reduced considerably. This LPI technique is expanded for the case of a two-dimensional antenna array. With this added dimension, the computational complexity of the method is increased, as the pattern now changes with respect to both θ and ϕ. Simulation results show that the developed technique is still applicable for a two-dimensional array. A carefully calculated set of complex coefficients can be applied across the set of low-gain basis patterns, which are simply the high-gain patterns spoiled by a certain phase shift, in a weighted summation. The results of this summation can be shown to provide nearly identical returns when compared to that of a traditional high-gain single beam scanned across the observation area. The high-gain transient power is replaced by lower power signals with an increased integration time, resulting in the same total energy on the target, and thus the same

detection performance. The simulation results show that the intercept area, the area in which a hostile intercept receiver can detect the transmitted signal, can be reduced significantly due to the low gain of the transmitted spoiled patterns. For example, the intercept area is reduced by as much as 96% in the case of a 32x32 element array. The LPI benefits of this technique - significantly reducing the range at which a hostile receiver can intercept the radar beam while maintaining the range at which the radar can detect the target - are of obvious benefit in the ongoing battle of electronic warfare.

Acknowledgments

First and foremost, I owe everything to God for all he has done for me. He has blessed my life tremendously by allowing me to attend Auburn University for both my undergraduate and graduate degrees.

I credit Daniel Lawrence for developing and publishing the novel approach explored in this thesis. I would like to thank him for allowing me to expand his work for my thesis and for the assistance he provided in that process.

I would like to thank Dr. Lloyd Riggs for being my advisor, for his aid in this research and for his support throughout my undergraduate and graduate years. In addition, I thank the other members serving on my advising committee: Dr. Baginski, Dr. Wentworth, and Dr. Wang.

I would like to express my gratitude to the many faculty members in the Department of Electrical Engineering at Auburn University who have taught and advised me during my time at Auburn. Their teaching and guidance have equipped me with the tools necessary to succeed both academically and professionally.

I would like to thank Kevin Nash and Pete Kirkland for the valuable work experience they provided during my years working at SMDC as a coop student. This work, and their mentoring, introduced me to the field of radar analysis which provided focus for my graduate studies.

Finally, I wish to thank my parents, Ed and Melinda Goad, for raising me in a Godly home and for homeschooling me for twelve years. They equipped me academically and instilled within me a work ethic that has allowed me to pursue my academic goals successfully.

Table of Contents

List of Figures

Chapter 1

Introduction

On the modern battlefield, radar systems have become a vital component of warfare and can provide a significant military advantage to whoever possesses them. There are many critical uses of radar systems including both active and passive surveillance and detection for offensive purposes. These radar systems can assume many different shapes and forms and can be mounted on a wide range of platforms such as missiles, aircraft, and sea and land based observation platforms. Regardless of location, purpose, and scope, however, all radar systems share a high vulnerability to detection and exploitation by opposing systems.

1.1 Background

1.1.1 Electronic Warfare

The term electronic warfare (EW) is used to classify military action to identify, prevent, or exploit hostile use of the electromagnetic spectrum. EW can be further divided into two categories: electronic support measures and electronic countermeasures. Electronic support measures (ESM) involve actions taken to search for, identify, and analyze detected radar signals. Although ESM are by definition passive, they can provide a source of EW information required to conduct counter measures. Electronic counter measures (ECM) involve actions taken to prevent or reduce hostile use of the electromagnetic spectrum, or actions that actively seek to exploit the hostile radar system. A further distinction, electronic counter-countermeasures (ECCM) involves actions taken to ensure friendly use of the electromagnetic spectrum despite hostile ECM efforts [1].

1.1.2 Growing ECM Threat

The increasing prevalence of ESM and ECM systems poses a great threat to any system relying on radar performance. For example, aircraft often face great risk from enemy defenses if they are detected by hostile ESM or ECM systems. Stationary radar systems also face threats from Anti-Radiation Missiles (ARM). The threat posed by these missiles has two aspects that must be considered. First, it is to the advantage of the radar to avoid for as long as possible any reconnaissance of hostile ARM or ECM systems. Second, in order to protect itself from incoming missiles, the radar must work to deceive the ARM without interrupting search operations [2].

The operation of a radar system can also be severely hampered by noise jamming and deception jamming efforts by ECM systems. Noise jamming involves deliberate radiation in order to disturb the normal operation of a radar, while deception jamming involves an attempt to deceive the radar using methods such as range deception or velocity deception [3].

Due to the great risk associated with these threats, it should be a goal of every radar design facing these dangers to attempt in some capacity to avoid detection by a hostile system. The steps in the deployment of an ECM system can be listed as follows:

1. Search in frequency, azimuth, and elevation
2. Detect an incoming radar signal
3. Identify the signal by its emission characteristics and assess priority of the signal
4. Select the proper ECM to employ
5. Initiate the ECM operation

Any delay in any of these steps could prevent timely ECM initiation, providing an advantage to the detected system; therefore, it is beneficial to design radar systems

with ECCM properties in an attempt to decrease the threat caused by hostile systems [4].

1.2 Introduction to Low Probability of Intercept

Because of the increased threat of ESM and ECM systems, a great focus has been placed on developing radar systems designed to combat the dangers of detection. Known as low probability of intercept (LPI) radar systems, these sensors have been designed to reduce the potential for detection and exploitation by ESM and ECM systems.

1.2.1 Inherent Weakness of Monostatic Radars

An inherent weakness of any monostatic radar system attempting to avoid detection by an intercept receiver involves the difference in propagation loss between the radar and the receiver. The theoretical performance of such a radar system can be defined by the radar range equation [5]. For one way propagation of a transmitted beam, the power density Q_i at a point at a distance R away from the transmitting source can be calculated as

$$Q_i = \frac{P_t G_t}{4\pi R^2} \tag{1.1}$$

The power reflected by the target back towards the radar can be expressed by the product of the incident power density and the radar cross section, σ, of the target. When considering radar propagation, this reflected power must be taken into account to compensate for the propagation losses of the wave travelling to the target and back to the transmitter. The resulting power density Q_r received at the transmitter can be calculated as

$$Q_r = \frac{P_{refl}}{4\pi R^2} = \frac{P_t G_t \sigma}{(4\pi)^2 R^4} \tag{1.2}$$

From these equations, it can be seen that while one-way propagation loss is proportional to $1/R^2$, two-way propagation loss is proportional to $1/R^4$, meaning that the power received by a radar system is reduced by the power seen by the target by a factor of $1/R^2$. This difference benefits the ESM receiver greatly, as it will always have the advantage over the radar in terms of received power. In strategic terms, this means that the intercept receiver in most cases will be able to detect the signal of the radar system before it itself is detected.

1.2.2 Goal of LPI Development

It is important to note that, as active sensors, all traditional radar systems must have a finite probability of intercept [6]. That is, there is always a minimum range between the radar and the ESM system where the detection threshold of the intercepting receiver is exceeded. Therefore, it is not a feasible goal to completely avoid detection by a hostile system, but rather to delay that detection as long as possible. The quiet range of a radar can be defined as the range that the radar can detect a target without interception from a hostile ESM system [7]. The primary underlying goal of LPI, therefore, is to focus on increasing this range as much as is practical for a given radar system.

1.3 Existing LPI Techniques

In order to overcome the inherent disadvantage of a radar system due to propagation losses, a number of techniques have been developed to attempt to reduce the visibility of the radar to any hostile ESM systems to enhance LPI performance. One of the primary methods of reducing the visibility of a radar system involves spreading the transmitted energy, either over time, frequency, or space. It should be noted that technically there exists a distinction between such spread spectrum techniques and true low probability of intercept techniques [8]. The principal idea of true LPI radar

is to avoid interception by mismatching the waveform of the radar with the waveforms that the ESM system is expecting to receive. As a result, the development of such a system requires the designer to consider the ESM and ECM systems the radar wishes to avoid, and a complete assessment of the LPI performance must include analysis of both the radar and the hostile systems [7]. Although this technical distinction between approaches exists, the term LPI is used universally to describe any system attempting to reduce its probability of intercept by a hostile system.

1.3.1 Reducing Transmitted Energy Density

As mentioned above, in general the capacity to reduce the visibility of a radar system involves reducing the energy density of the transmitted signal. This can be accomplished by spreading the energy over a longer time by using high duty cycle, or even continuous wave, waveforms, spreading it over a wider bandwidth, or spreading it in space, reducing the transmit antenna gain by spreading the energy over a wider angle [6]. Although there are many ways to implement these spreading techniques, the concept of high duty cycle, wideband waveforms is generally accepted as advantageous to reducing visibility. By increasing the time duration of a waveform, the peak power can be lowered while maintaining the same average power. By increasing the bandwidth of the waveform, the power spectral density can be lowered, reducing the probability of narrowband interception [9]. According to [10], one of the most effective techniques for reducing the probability of detection by an ESM system is to implement ultra wide bandwidth pulses, causing the radar's transmitted signal to be mismatched to what the intercept receiver is expecting.

The authors of [11] discuss the many advantages of wideband radars, which include providing better target identification, and a greater reliability of detection. They can also provide better velocity tracking, as the accuracy of wideband measurements is less affected by target maneuvering than narrowband measurements.

Wideband radars can also provide better secrecy and electromagnetic compatibility, and also allow some level of immunity from interference; since the signal energy is distributed through the spectrum, any jamming signal must be distributed as well, requiring significantly more power to effectively maintain jamming capability. However, it is also noted in [11] that excessive widening of the signal bandwidth can lead to a decrease in detection quality if the bandwidth is increased such that individual scatterers on the target are resolved in range.

1.3.2 Continuous Wave Radar

As discussed above, waveforms with high duty cycle or pulse repetition frequency (PRF) allow the transmitted energy to be spread over time, resulting in increased LPI performance. The PRF of a waveform could be increased to the extreme case of becoming a continuous-wave (CW) transmission. A significant advantage of a CW system is the ease and accuracy with which such systems are able to process Doppler shifts. A disadvantage of CW radars, however, is their inability to measure range. One solution to this deficiency is the frequency modulated continuous-wave (FMCW) radar, which generates a range beat by changing the transmitter frequency [12]. FMCW is a simple way of giving a radar an extremely high time bandwidth product. This results in a high resistance to interception by ESM systems, due the impracticality of matching the ESM receiver to the radar's sweep pattern or effectively jamming the system [13].

Many believe that a CW waveform is the ideal waveform for LPI radar, as the peak power of such a system is much lower than that of a pulsed radar. Although the advantages of a CW, or FMCW, waveform are great, these systems also face certain limitations. CW systems can be either monostatic, meaning a single antenna for both transmit and receive, or bistatic, with separate antennas. Monostatic systems suffer

from leakage due to transmitting and receiving simultaneously. A bistatic arrangement eliminates this problem by separating the transmit and receive antennas by some distance; however, this separation introduces other issues, such as the difficulty in correctly synchronizing time and direction between the two antennas [14].

1.3.3 Noise Radar

LPI development in radar systems with pulse or chirp waveforms is becoming increasingly difficult, as these waveforms are so well defined and therefore are easier to exploit with ESM systems. As a result, some researchers have begun focusing on the development of noise radars. Also known as random signal radars, these are systems whose transmitting signal is modulated by a lower frequency noise, or is itself microwave noise [15]. An ideal noise waveform is random by nature, resulting in a nonperiodic waveform. This makes interception extremely difficult, as each successive pulse is uncorrelated [16]. It has been shown in [17] that both phase and frequency modulated noise radar can result in a wider output bandwidth and sidebands that are suppressed significantly more than the modulated signal of a traditional radar system.

Random signal radars often work in continuous-wave mode. This is due to the advantanges of CW radar over conventional pulsed radar in regards to LPI performance, and also the ease with which random signal radar can be operated in CW mode. However, the inherent disadvantages of CW radar, such as leakage in the case of a monostatic setup, also apply to these random signal radars. This leakage, and its constraing on operating range, can be the most difficult weakness to overcome when developing random signal radars [15].

1.3.4 Frequency Hopping

Another area of research involves frequency hopping. If the total illumination time on a target is longer than the coherent processing interval required by the radar, the carrier frequency of the transmitted signal may be changed to allow a new coherent processing interval to begin. Such frequency agility greatly increases the difficulty of interception by an ESM system, as the interceptor receiver must now cover the entire frequency band implemented by the radar [18]. Much research has been done and many papers have been written on development in this area, such as techniques based on the application of spread spectrum-frequency hopping methods [19], and modulators for burst-by-burst carrier frequency hopping in TDMA systems [20].

1.3.5 Other Methods

Many other methods exist to reduce visibility and enhance LPI performance. In [21], a novel approach has been proposed involving antenna hopping. In this paper, the author argues that frequency or phase modulation can be imposed on a signal by the phase shift resulting from switching either receiver input or the transmitter output among a set of antennas. Some researchers, seeing a potential need for radars without a scanning transmit main beam, have developed what are known as omnidirectional radars. These systems, such as the one discussed in [2], require the transmitter to illuminate the search area continuously, due to the lack of a main scanning beam. Although these systems have very low transmit gain, they are dependent upon multiple receiving beams to provide continuous coverage of the observation space.

1.4 A Novel Approach to LPI

In [22], a novel technique is developed to provide low probability of interception for radar systems with phased array antennas. This method involves replacing the traditional high-gain antenna beam used to scan a search region with a weighted

summation of a set of low-gain, "spoiled" beams. These spoiled beams are created by simply adding a certain phase shift pattern across the array to reduce gain; thus, this technique could in theory be applied to an existing array with minimal modifications. The goal of this technique is to reduce the peak gain of the transmitted pattern while maintaining the same performance as a traditional scanned radar system with a high-gain main beam. It should be noted that this method is not designed to increase the quiet gain of the radar, that is, the range at which the radar can detect a target without interception from a hostile ESM system; therefore, such a system still has no guarantee of being able to detect a target before being detected itself. Rather, the technique simply aims to reduce as much as possible the intercept range of an ESM receiver, thus reducing the probability of intercept. It can be shown using (1.1) that a reduction of 10 dB in the gain of the transmitting antenna reduces the maximum intercept range of the ESM system by a factor of $1/\sqrt{10}$. This translates into a 90% reduction in the intercept area of the ESM receiver. If the detection range and performance of the transmitting radar can be maintained while also drastically reducing the intercept range of any potential hostile ESM systems, then the LPI benefits of such a technique would be substantial. The author of [22] claims to accomplish this feat by effectively replacing the traditional high gain transient sweep with lower power beams radiated persistently over the observation area, as demonstrated in the following chapter.

Chapter 2

Original LPI Approach

In [22], the author develops a beam-spoiling technique designed to increase LPI performance of a radar system. The main approach of this method involves sequentially forming a series of low-gain spoiled beams over the desired search area instead of scanning with a single high-gain transmit beam. The author claims that after transmitting and receiving the spoiled beams, the set of formed low-gain beams can be weighted and combined to achieve the same detection results as a single high-gain beam, effectively replacing high transmit power with increased scan times. This technique would reduce the peak power radiated in any one direction while still maintaining the same antenna performance as a traditional scanned radar system.

2.1 Theoretical Development of the Original Approach

The high-gain pattern synthesis approach presented in [22] applies to a one-dimensional linear phased antenna array, as shown in Figure 2.1. The far-field radiation pattern of such an array with N elements can be expressed as

$$f_0(\theta) = 1 + e^{j\beta d \sin(\theta)} + e^{j2\beta d \sin(\theta)} + ... + e^{j(N-1)\beta d \sin(\theta)} \tag{2.1}$$

where $\beta = 2\pi/\lambda$ is the free-space propagation constant, d is the array element spacing, and θ is the spatial angle measured from the broadside direction. To reduce the complexity of the calculations, it is beneficial to make the substitution $\psi = \beta d \sin(\theta)$. If θ varies from -90° to 90°, then ψ will vary from $-j\beta d$ to $j\beta d$. The step size of this array will determine the precision of the array pattern. In [22], d is set at one half

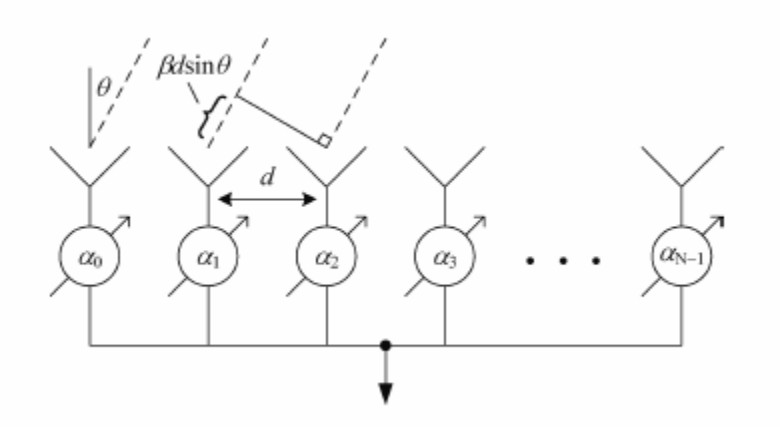

Figure 2.1: N-element linear phased array antenna

of a wavelength ($d = \lambda/2$), but because of the substitution of ψ into the equations, the element spacing and frequency can be changed without increasing the complexity of the mathematics. With the substitution, the fundamental array pattern can be rewritten as

$$f_0(\psi) = 1 + e^{j\psi} + e^{j2\psi} + \cdots + e^{j(N-1)\psi} \tag{2.2}$$

This array pattern results in a main lobe with high gain directed broadside to the array. This main lobe can be scanned by applying a linear phase progression across the elements of the array. In [22], a phase scan of $\gamma = 2\pi/N$ is selected. This allows a total of N scanned patterns to be produced; that is, N distinct far-field patterns exist with the center of the main lobe pointing in N even increments between $-90°$ and $90°$. The number of scanned patterns, and hence the density of the scanned area, can either be increased or reduced as desired by changing the value of N in γ. The

set of scanned patterns can be written as

$$\begin{aligned} f_1(\psi) &= 1 + e^{j\gamma}e^{j\psi} + e^{j2\gamma}e^{j2\psi} + \cdots + e^{j(N-1)\gamma}e^{j(N-1)\psi} \\ f_2(\psi) &= 1 + e^{j2\gamma}e^{j\psi} + e^{j4\gamma}e^{j2\psi} + \cdots + e^{j2(N-1)\gamma}e^{j(N-1)\psi} \\ &\vdots \\ f_{N-1}(\psi) &= 1 + e^{j(N-1)\gamma}e^{j\psi} + \cdots + e^{j(N-1)(N-1)\gamma}e^{j(N-1)\psi} \end{aligned} \tag{2.3}$$

For purposes of LPI applications, it is desirable to reduce the peak power transmitted in any one direction to reduce the potential for detection by ECM systems, while still maintaining the same range and coverage. The author of [22] proposes that this can be accomplished by creating a set of low-gain, spoiled basis patterns which can then be weighted and combined to form a far-field pattern with gain equivalent to that of the original fundamental array pattern. For optimal performance in this scheme, the low-gain patterns should have low gain and broad beamwidth. It is possible to create such a spoiled beam by applying a certain phase shift to each element of the array. In [22], a quadratic phase shift, shown in Figure 2.2, is applied across the elements of the array used to create the low gain pattern. This phase shift pattern both defocuses the beam and reduces the gain of the array.

Such an antenna array pattern can be expressed as

$$g_0(\psi) = 1 + e^{j\alpha_1}e^{j\psi} + e^{j\alpha_2}e^{j2\psi} + \cdots + e^{j\alpha_{N-1}}e^{j(N-1)\psi}, \tag{2.4}$$

where $\alpha_1, \alpha_2, \ldots \alpha_{N-1}$ are shown in Figure 2.2. When comparing (2.2) and (2.4), it is obvious that the basis pattern g_0 is simply the fundamental pattern f_0 "spoiled" by applying the phase shift pattern. Figure 2.3 shows the fundamental array pattern g_0 and the fundamental basis pattern f_0. In these simulations, the gain of the main lobe

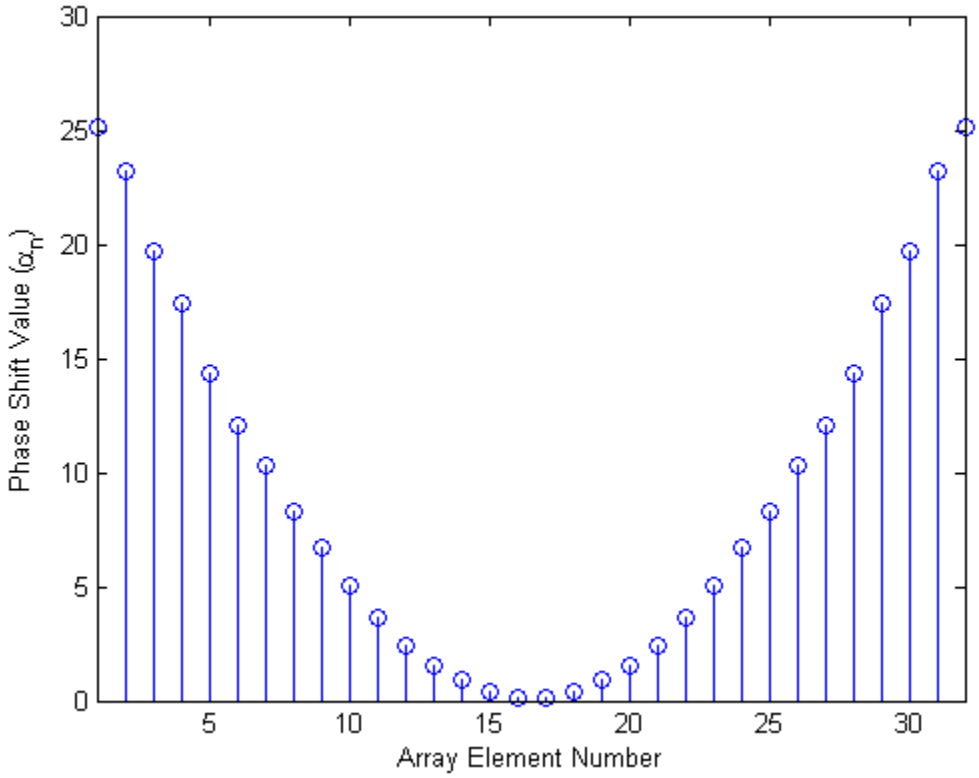

Figure 2.2: Quadratic Phase Shift

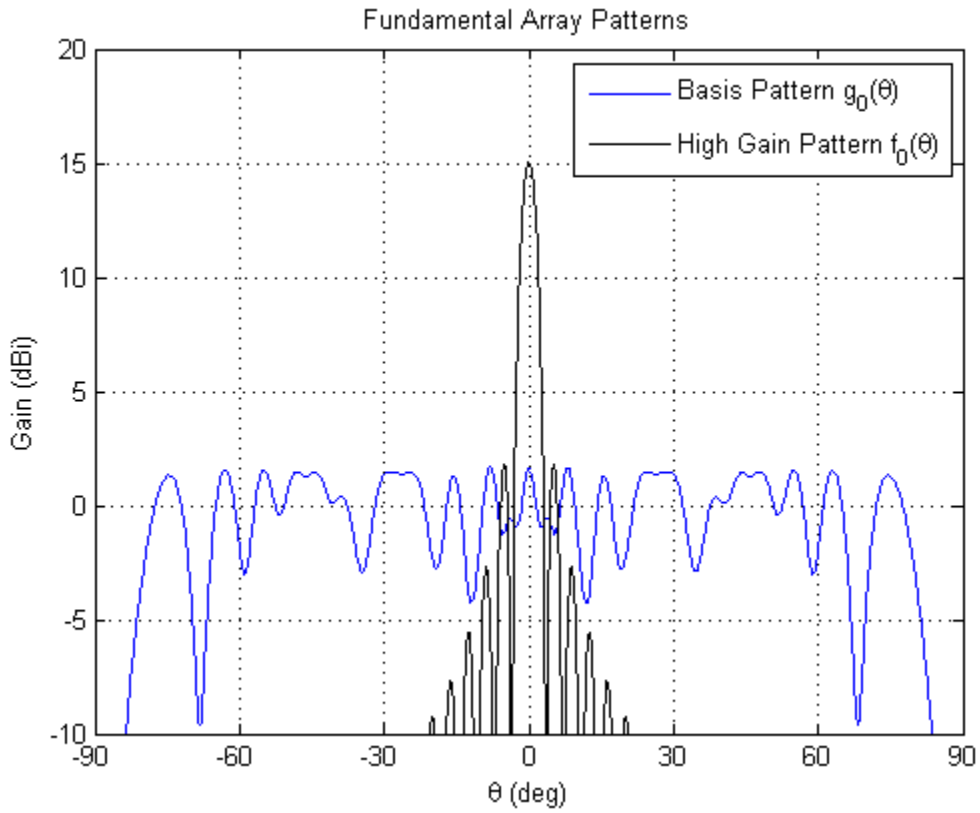

Figure 2.3: Fundamental Array Pattern and Basis Pattern

of the f_0 is approximately 15 dB, while the maximum gain of g_0 is approximately 1.7 dB.

As in the case of the fundamental array pattern, a set of N low-gain patterns can be formed by applying the same linear phase progression, which can be written as

$$\begin{aligned} g_1(\psi) &= 1 + e^{j\alpha_1}e^{j\gamma}e^{j\psi} + \cdots + e^{j\alpha_{N-1}}e^{j(N-1)\gamma}e^{j(N-1)\psi} \\ g_2(\psi) &= 1 + e^{j\alpha_1}e^{j2\gamma}e^{j\psi} + \cdots + e^{j\alpha_{N-1}}e^{j2(N-1)\gamma}e^{j(N-1)\psi} \\ &\vdots \\ g_{N-1}(\psi) &= 1 + e^{j\alpha_1}e^{j(N-1)\gamma}e^{j\psi} + \cdots + e^{j\alpha_{N-1}}e^{j(N-1)(N-1)\gamma}e^{j(N-1)\psi} \end{aligned} \tag{2.5}$$

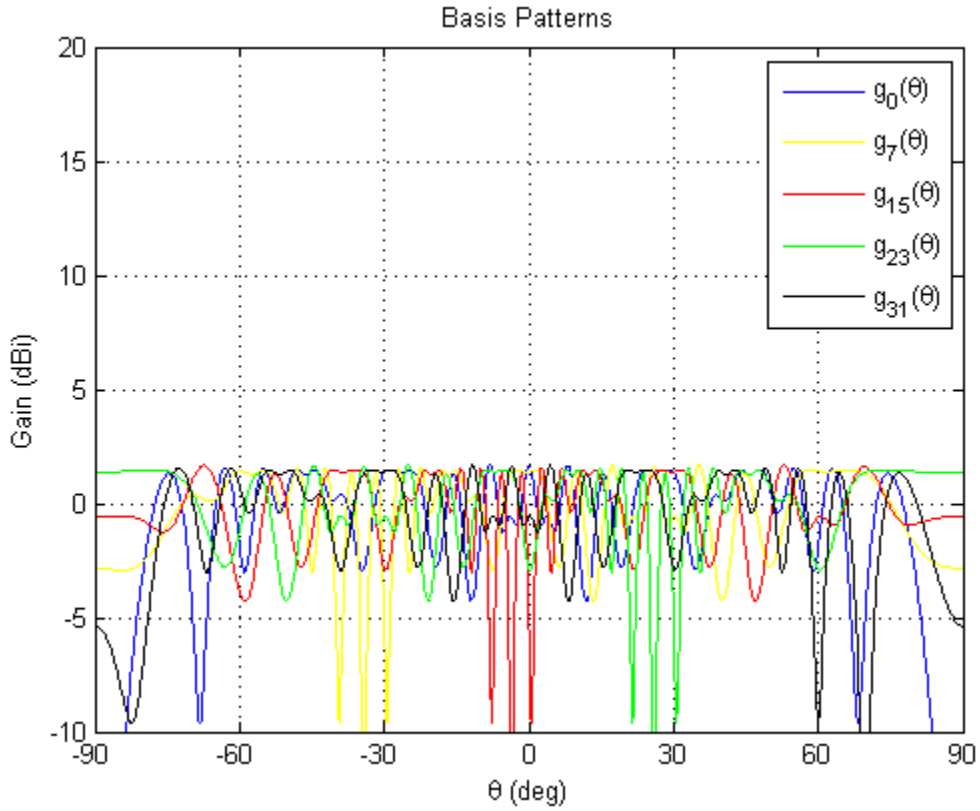

Figure 2.4: Basis Patterns

Again, when comparing (2.3) and (2.5), it is apparent that the set of basis patterns are simply the equivalent steered patterns spoiled by the phase shift pattern shown in Figure 2.2. As a result, each basis pattern g_n is steered to a specific angle of θ, just as the original steered pattern; however, due to the spoiling effect of the applied phase shift, the gain of the main lobe is reduced, resulting in the patterns shown in Figure 2.4. Although steered to different angles, the set of basis patterns appear to be indistinguishable because of the spoiling effect.

If it is assumed that the original fundamental array pattern can be written as a linear combination of the set of basis patterns, then the reconstructed pattern can be written as

$$f_0(\psi) = \omega_{0,0}g_0(\psi) + \omega_{0,1}g_1(\psi) + \omega_{0,2}g_2(\psi) + \cdots + \omega_{0,N-1}g_{N-1}(\psi) \qquad (2.6)$$

$\omega_(0, n)$ represents the weighting of each basis pattern that is required for the sum of the basis patterns to have a far-field pattern equivalent to that of the fundamental array. This process can be extended to reconstruct all N possible array patterns from (2.3) as follows

$$\begin{aligned}
f_1(\psi) &= \omega_{1,0}g_0(\psi) + \omega_{1,1}g_1(\psi) + \omega_{1,2}g_2(\psi) + \cdots + \omega_{1,N-1}g_{N-1}(\psi) \\
&= 1 + e^{j\gamma}e^{j\psi} + e^{j2\gamma}e^{j2\psi} + \cdots + e^{j(N-1)\gamma}e^{j(N-1)\psi} \\
f_2(\psi) &= \omega_{2,0}g_0(\psi) + \omega_{2,1}g_1(\psi) + \omega_{2,2}g_2(\psi) + \cdots + \omega_{2,N-1}g_{N-1}(\psi) \\
&= 1 + e^{j2\gamma}e^{j\psi} + e^{j4\gamma}e^{j2\psi} + \cdots + e^{j2(N-1)\gamma}e^{j(N-1)\psi} \\
&\vdots \\
f_{N-1}(\psi) &= \omega_{N-1,0}g_0(\psi) + \omega_{N-1,1}g_1(\psi) + \omega_{N-1,2}g_2(\psi) + \cdots + \omega_{N-1,N-1}g_{N-1}(\psi) \\
&= 1 + e^{j(N-1)\gamma}e^{j\psi} + \cdots + e^{j(N-1)(N-1)\gamma}e^{j(N-1)\psi}
\end{aligned} \tag{2.7}$$

In order to calculate the needed weights, a matrix equation can be set up by equating the equal powers of $e^{j\psi}$ of the high-gain patterns and basis patterns. For example, for the fundamental pattern $f_0(\psi)$, an equation can be set up to find the coefficients $\omega_{0,n}$

$$A \cdot \begin{bmatrix} \omega_{0,0} \\ \omega_{0,1} \\ \omega_{0,2} \\ \vdots \\ \omega_{0,N-1} \end{bmatrix} = \begin{bmatrix} 1 \\ 1 \\ 1 \\ \vdots \\ 1 \end{bmatrix} \tag{2.8}$$

where the matrix A is defined in (2.9).

$$A = \begin{bmatrix} 1 & 1 & 1 & & 1 \\ e^{j\alpha_1} & e^{j(\alpha_1+\gamma)} & e^{j(\alpha_1+2\gamma)} & \cdots & e^{j(\alpha_1+(N-1)\gamma)} \\ e^{j\alpha_2} & e^{j(\alpha_1+2\gamma)} & e^{j(\alpha_2+4\gamma)} & & e^{j(\alpha_1+(N-1)\gamma)} \\ & \vdots & & \ddots & \vdots \\ e^{j\alpha_{N-1}} & e^{j(\alpha_{N-1}+(N-1)\gamma)} & e^{j(\alpha_{N-1}+2(N-1)\gamma)} & \cdots & e^{j(\alpha_{N-1}+(N-1)(N-1)\gamma)} \end{bmatrix} \quad (2.9)$$

Similar matrix equations can be set up relating each of the scanned beams to the set of basis patterns, resulting in a total of N scanned beams

$$
\begin{aligned}
A \cdot \begin{bmatrix} \omega_{1,0} \\ \omega_{1,1} \\ \omega_{1,2} \\ \vdots \\ \omega_{1,N-1} \end{bmatrix} &= \begin{bmatrix} 1 \\ e^{j\gamma} \\ e^{j2\gamma} \\ \vdots \\ e^{j(N-1)\gamma} \end{bmatrix} \\
A \cdot \begin{bmatrix} \omega_{2,0} \\ \omega_{2,1} \\ \omega_{2,2} \\ \vdots \\ \omega_{2,N-1} \end{bmatrix} &= \begin{bmatrix} 1 \\ e^{j2\gamma} \\ e^{j4\gamma} \\ \vdots \\ e^{j2(N-1)\gamma} \end{bmatrix} \\
&\vdots \\
A \cdot \begin{bmatrix} \omega_{N-1,0} \\ \omega_{N-1,1} \\ \omega_{N-1,2} \\ \vdots \\ \omega_{N-1,N-1} \end{bmatrix} &= \begin{bmatrix} 1 \\ e^{j(N-1)\gamma} \\ e^{j2(N-1)\gamma} \\ \vdots \\ e^{j(N-1)(N-1)\gamma} \end{bmatrix}
\end{aligned}
\tag{2.10}
$$

These equations can then be combined into a single matrix equation to solve for all the coefficients simultaneously

$$\begin{bmatrix} \omega_{0,0} & \omega_{1,0} & \omega_{2,0} & & \omega_{N-1,0} \\ \omega_{0,1} & \omega_{1,1} & \omega_{2,1} & \cdots & \omega_{N-1,1} \\ \omega_{0,2} & \omega_{1,2} & \omega_{2,2} & & \omega_{N-1,2} \\ & \vdots & & \ddots & \vdots \\ \omega_{0,N-1} & \omega_{1,N-1} & \omega_{2,N-1} & \cdots & \omega_{N-1,N-1} \end{bmatrix}$$

$$= A^{-1} \cdot \begin{bmatrix} 1 & 1 & 1 & & 1 \\ 1 & e^{j\gamma)} & e^{j2\gamma} & \cdots & e^{j(N-1)\gamma} \\ 1 & e^{j2\gamma)} & e^{j4\gamma} & & e^{j2(N-1)\gamma} \\ & \vdots & & \ddots & \vdots \\ 1 & e^{j(N-1)\gamma)} & e^{j2(N-1)\gamma} & \cdots & e^{j(N-1)(N-1)\gamma} \end{bmatrix} \quad (2.11)$$

The complex coefficient weights found allow high-gain patterns to be formed by linear combinations of the N spoiled beams. Once these weights have been calculated, all N of the steered high-gain patterns can be synthesized at once. Figure 2.5 shows the reconstructed high-gain patterns steered to 0 deg, +30 deg, and -30 deg.

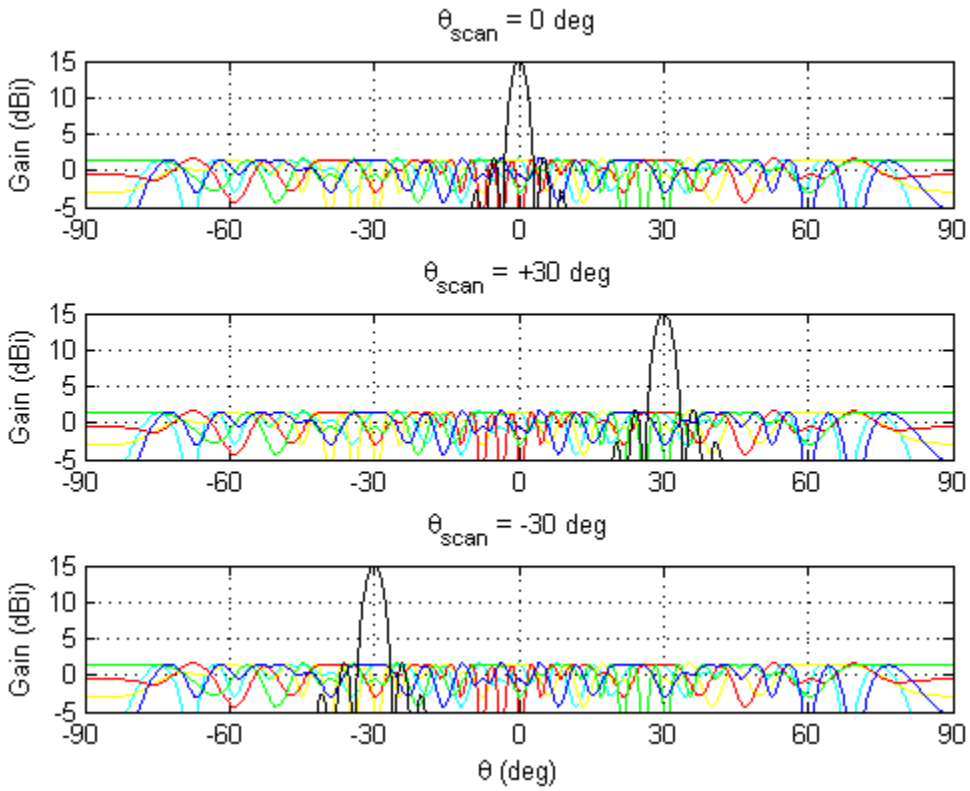

Figure 2.5: Scanned Patterns

Chapter 3

Expansion of the 2D Method Into 3D

Although the method developed in the previous chapter has obvious benefits for designing a LPI method of beamforming, a one-dimensional antenna array design, which can only point in one plane, is not practical for a real world radar system. Therefore, it is beneficial to explore whether this technique can be expanded into three dimensions. In order to create a far-field array pattern that is scannable in both directions, a two-dimensional antenna array must be used instead of the original one-dimensional array. The analysis for the two-dimensional array follows the same theory as for the one-dimensional array; however, each element now has radiation components in both the x and y planes, represented by θ and ϕ, respectively. Similarly to the case of the one-dimensional array, we can make the substitutions $\psi_n = \beta d \sin(\theta)$ and $\psi_m = \beta d \sin(\phi)$. Throughout this theoretical development, n represents the rows of the array of N elements, while m represents the columns of the array of M elements. If the range $-90^\circ \leq \theta \leq 90^\circ$ and $-90^\circ \leq \phi \leq 90^\circ$ is considered, then both ψ_n and ψ_m will vary from $-j\beta d$ to $j\beta d$, with the step size determining the precision of the array pattern. This antenna configuration and range of angles allows the creation of a far-field array pattern that can be scanned to any point over a the hemisphere in front of the array.

3.1 Theoretical Calculations

Allowing for changes in both θ and ϕ, the fundamental array pattern of a NxM two-dimensional array can be written as

$$\begin{aligned} f_0(\theta,\phi) &= 1 + e^{j\beta d\sin(\theta)}e^{j\beta d\sin(\phi)} + e^{j2\beta d\sin(\theta)}e^{j2\beta d\sin(\phi)} + \\ &\quad ... + e^{j(N-1)\beta d\sin(\theta)}e^{j(N-1)\beta d\sin(\phi)} \\ &= \sum_{n=0}^{N-1}\sum_{m=0}^{M-1} e^{jn\psi_n}e^{jm\psi_m} \end{aligned} \tag{3.1}$$

As in the case of the one-dimensional antenna array, a linear phase progression can be applied across the array to steer the main lobe. If this phase scan is selected to be $\gamma = 2\pi/N$,the a total of NM scanned beams can be formed, with N beam pointing angles in θ and M beam pointing angles in ϕ. It should be noted that this selection of the phase scan is made for convenience in showing the equations involved in developing the technique. The value of γ, and thus the scanning angle increment, can be changed with only minor modifications to the equations developed below. The linear phase progression can be applied across the elements of the two-dimensional array as follows: First, an increasing phase progression of γ will be applied incrementally across the rows of the array only, resulting in N beam formations that vary only in θ. A phase of γ will then be applied across the columns of the array, and the same increasing phase progression will be applied across the rows to create another N beams formations. This process will be repeated M times until a total of NM beam formations have

been created. The set of scanned beams can be represented as

$$
\begin{aligned}
f_1(\psi_n,\psi_m) &= \sum_{n=0}^{N-1}\sum_{m=0}^{M-1} e^{jn(\psi_n+\gamma)}e^{jm\psi_m} \\
f_2(\psi_n,\psi_m) &= \sum_{n=0}^{N-1}\sum_{m=0}^{M-1} e^{jn(\psi_n+2\gamma)}e^{jm\psi_m} \\
f_3(\psi_n,\psi_m) &= \sum_{n=0}^{N-1}\sum_{m=0}^{M-1} e^{jn(\psi_n+3\gamma)}e^{jm\psi_m} \\
&\vdots \\
f_{N-1}(\psi_n,\psi_m) &= \sum_{n=0}^{N-1}\sum_{m=0}^{M-1} e^{jn(\psi_n+(N-1)\gamma)}e^{jm\psi_m} \\
f_N(\psi_n,\psi_m) &= \sum_{n=0}^{N-1}\sum_{m=0}^{M-1} e^{jn\psi_n}e^{jm(\psi_m+\gamma)} \\
f_{N+1}(\psi_n,\psi_m) &= \sum_{n=0}^{N-1}\sum_{m=0}^{M-1} e^{jn(\psi_n+\gamma)}e^{jm(\psi_m+\gamma)} \\
&\vdots \\
f_{N^2-1}(\psi_n,\psi_m) &= \sum_{n=0}^{N-1}\sum_{m=0}^{M-1} e^{jn(\psi_n+(N-1)\gamma)}e^{jm(\psi_m+(N-1)\gamma)}
\end{aligned}
\tag{3.2}
$$

Now, the same assumption from the one-dimensional case is made: that the above high-gain patterns can be created from a weighted combination of low-gain, spoiled basis patterns. These basis patterns are similar to the basis patterns developed for the two-dimensional array, except that now they must account for changes in the x and y planes. Also, a new set of phase shifts must be developed for the two-dimensional array. Again, each element will have a certain phase shift $\alpha_{n,m}$ applied to it, with the ultimate goal of creating a defocused, spoiled far-field pattern. The selection of the values of α is discussed further in Section 3.2. The fundamental basis pattern can be

written as

$$\begin{aligned} g_0(\theta,\phi) =& 1 + e^{j\alpha_{0,1}} e^{j\beta d \sin(\theta)} e^{j\beta d \sin(\phi)} + e^{j\alpha_{0,2}} e^{j2\beta d \sin(\theta)} e^{j2\beta d \sin(\phi)} + ... \\ & + e^{j\alpha_{N-1,N-1}} e^{j(N-1)\beta d \sin(\theta)} e^{j(N-1)\beta d \sin(\phi)} \\ =& \sum_{n=0}^{N-1} \sum_{m=0}^{M-1} e^{j\alpha_{n,m}} e^{jn\psi_n} e^{jm\psi_m} \end{aligned} \tag{3.3}$$

Again, it should be noted that the only difference between this pattern and the fundamental array pattern from (3.2) is the extra phase shift $\alpha_{n,m}$, which serves to spoil the high gain beam pattern. As in the case of the high-gain array patterns, a set of N^2 low-gain basis patterns can be formed by applying a linear phase progression γ across the elements of the array. The application of γ follows the same pattern used for the high-gain patterns: incrementing the phase progression applied across

the rows, and then the columns, as observed in the following

$$
\begin{aligned}
g_1(\psi_n, \psi_m) &= \sum_{n=0}^{N-1} \sum_{m=0}^{M-1} e^{j\alpha_{0,1}} e^{jn(\psi_n+\gamma)} e^{jm\psi_m} \\
g_2(\psi_n, \psi_m) &= \sum_{n=0}^{N-1} \sum_{m=0}^{M-1} e^{j\alpha_{0,2}} e^{jn(\psi_n+2\gamma)} e^{jm\psi_m} \\
g_3(\psi_n, \psi_m) &= \sum_{n=0}^{N-1} \sum_{m=0}^{M-1} e^{j\alpha_{0,3}} e^{jn(\psi_n+3\gamma)} e^{jm\psi_m} \\
&\vdots \\
g_{M-1}(\psi_n, \psi_m) &= \sum_{n=0}^{N-1} \sum_{m=0}^{M-1} e^{j\alpha_{0,M}} e^{jn(\psi_n+(N-1)\gamma)} e^{jm\psi_m} \\
g_M(\psi_n, \psi_m) &= \sum_{n=0}^{N-1} \sum_{m=0}^{M-1} e^{j\alpha_{0,M}} e^{jn\psi_n} e^{jm(\psi_m+\gamma)} \\
g_{M+1}(\psi_n, \psi_m) &= \sum_{n=0}^{N-1} \sum_{m=0}^{M-1} e^{j\alpha_{0,M}} e^{jn(\psi_n+\gamma)} e^{jm(\psi_m+\gamma)} \\
&\vdots \\
g_{N^2-1}(\psi_n, \psi_m) &= \sum_{n=0}^{N-1} \sum_{m=0}^{M-1} e^{j\alpha_{N-1,N-1}} e^{jn(\psi_n+(N-1)\gamma)} e^{jm\psi_m+(N-1)\gamma}
\end{aligned} \tag{3.4}
$$

The equations for both the high-gain patterns and the low-gain patterns can be reduced to

$$
f_i(\psi_n, \psi_m) = \sum_{n=0}^{N-1} \sum_{m=0}^{M-1} e^{jn(\psi_n+a\gamma)} e^{jm(\psi_m+b\gamma)} \tag{3.5}
$$

$$
g_i(\psi_n, \psi_m) = \sum_{n=0}^{N-1} \sum_{m=0}^{M-1} e^{j\alpha_{m,n}} e^{jn(\psi_n+a\gamma)} e^{jm(\psi_m+b\gamma)} \tag{3.6}
$$

where

$$i = Na + b + 1$$

$$0 \leq a \leq N - 1$$

$$0 \leq b \leq M - 1$$

As before, the fundamental array pattern can be shown as a weighted combination of all N^2 basis patterns

$$\begin{aligned}
f_0(\theta,\phi) &= \omega_{0,0} g_0(\theta,\phi) + \omega_{0,1} g_1(\theta,\phi) + \cdots + \omega_{0,N^2-1} g_{N^2-1}(\theta,\phi) \\
f_1(\theta,\phi) &= \omega_{1,0} g_0(\theta,\phi) + \omega_{1,1} g_1(\theta,\phi) + \cdots + \omega_{1,N^2-1} g_{N^2-1}(\theta,\phi) \\
&\vdots \\
f_{N^2-1}(\theta,\phi) &= \omega_{N^2-1,0} g_0(\theta,\phi) + \omega_{N^2-1,1} g_1(\theta,\phi) + \cdots + \omega_{N^2-1,N^2-1} g_{N^2-1}(\theta,\phi)
\end{aligned} \tag{3.7}$$

Expanding the high-gain pattern and the basis patterns and equating equal powers of $e^{j\psi_n}$ and $e^{j\psi_m}$ allow the following matrix equation to be constructed for the coefficients required to recreate the fundamental array pattern f_0

$$A \cdot \begin{bmatrix} \omega_{0,0} \\ \omega_{0,1} \\ \omega_{0,2} \\ \vdots \\ \omega_{0,N^2-1} \end{bmatrix} = \begin{bmatrix} 1 \\ 1 \\ 1 \\ \vdots \\ 1 \end{bmatrix} \tag{3.8}$$

where A is defined in (3.9). The phase shifts applied to the rows and columns in this equation are represented by γ_n and γ_m, respectively. In this research, the phase applied across the rows and the columns are considered to be equal, i.e. $\gamma_n = \gamma_m$;

however, the separate phases are shown in (3.9) to aid in the explanation of the construction of the matrix A.

$$A = \begin{bmatrix} e^{j\alpha_{0,0}} & e^{j\alpha_{0,0}} & e^{j\alpha_{0,0}} & & e^{j\alpha_{0,0}} \\ e^{j\alpha_{0,1}} & e^{j(\alpha_{0,1}+\gamma_m)} & e^{j(\alpha_{0,1}+2\gamma_m)} & \dots & e^{j(\alpha_{0,1}+(N-1)\gamma_m)} \\ e^{j\alpha_{0,2}} & e^{j(\alpha_{0,2}+2\gamma_m)} & e^{j(\alpha_{0,2}+4\gamma_m)} & & e^{j(\alpha_{0,2}+2(N-1)\gamma_m)} \\ & \vdots & & & \vdots \\ e^{j\alpha_{0,N-1}} & e^{j(\alpha_{0,N-1}+(N-1)\gamma_m)} & e^{j(\alpha_{0,N-1}+2(N-1)\gamma_m)} & \dots & e^{j(\alpha_{0,N-1}+(N-1)(N-1)\gamma_m)} \\ e^{j\alpha_{1,0}} & e^{j\alpha_{1,0}} & e^{j\alpha_{1,0}} & \dots & e^{j(\alpha_{1,0}+(N-1)\gamma_n)} \\ e^{j\alpha_{1,1}} & e^{j(\alpha_{1,1}+\gamma_m)} & e^{j(\alpha_{1,1}+2\gamma_m)} & \dots & e^{j(\alpha_{1,1}+(N-1)\gamma_n+(N-1)\gamma_m)} \\ & \vdots & & & \vdots \\ e^{j\alpha_{N-1,N-1}} & e^{j(\alpha_{N-1,N-1}+(N-1)\gamma)} & e^{j(\alpha_{N-1,N-1}+2(N-1)\gamma)} & \dots & e^{j(\alpha_{N-1,N-1}+(N-1)(N-1)\gamma_n+(N-1)(N-1)\gamma_m)} \end{bmatrix} \tag{3.9}$$

This process can be repeated to form a total of N^2 matrix equations

$$
\begin{aligned}
A \cdot \begin{bmatrix} \omega_{1,0} \\ \omega_{1,1} \\ \omega_{1,2} \\ \vdots \\ \omega_{1,N^2-1} \end{bmatrix} &= \begin{bmatrix} 1 \\ e^{j\gamma} \\ e^{j2\gamma} \\ \vdots \\ e^{j(N-1)\gamma} \end{bmatrix} \\
A \cdot \begin{bmatrix} \omega_{2,0} \\ \omega_{2,1} \\ \omega_{2,2} \\ \vdots \\ \omega_{2,N-1} \end{bmatrix} &= \begin{bmatrix} 1 \\ e^{j2\gamma} \\ e^{j4\gamma} \\ \vdots \\ e^{j2(N-1)\gamma} \end{bmatrix} \\
&\vdots \\
A \cdot \begin{bmatrix} \omega_{N-1,0} \\ \omega_{N-1,1} \\ \omega_{N-1,2} \\ \vdots \\ \omega_{N-1,N-1} \end{bmatrix} &= \begin{bmatrix} 1 \\ e^{j(N-1)\gamma} \\ e^{j2(N-1)\gamma} \\ \vdots \\ e^{j2(N-1)(N-1)\gamma} \end{bmatrix}
\end{aligned}
\tag{3.10}
$$

The above matrix equations can be combined into a single N^2xN^2 matrix equation to solve for all equations simultaneously.

$$\begin{bmatrix} \omega_{0,0} & \omega_{1,0} & \omega_{2,0} & & \omega_{(N-1)^2,0} \\ \omega_{0,1} & \omega_{1,1} & \omega_{2,1} & \cdots & \omega_{(N-1)^2,1} \\ \omega_{0,2} & \omega_{1,2} & \omega_{2,2} & & \omega_{(N-1)^2,2} \\ & \vdots & & \ddots & \vdots \\ \omega_{0,(N-1)^2} & \omega_{1,(N-1)^2} & \omega_{2,(N-1)^2} & \cdots & \omega_{(N-1)^2,(N-1)^2} \end{bmatrix}$$

$$= A^{-1} \cdot \begin{bmatrix} 1 & 1 & 1 & & 1 \\ 1 & e^{j\gamma} & e^{j2\gamma} & \cdots & e^{j(N-1)\gamma} \\ 1 & e^{j2\gamma} & e^{j4\gamma} & & e^{j2(N-1)\gamma} \\ & \vdots & & \ddots & \vdots \\ 1 & e^{j(N-1)\gamma} & e^{j2(N-1)\gamma} & \cdots & e^{j2(N-1)(N-1)\gamma} \end{bmatrix} \quad (3.11)$$

As discussed in the analysis of the two-dimensional case, once the complex coefficients have been calculated, all N^2 steered patterns can be synthesized at once. Because the complex coefficients can be calculated prior to scanning, the performance of the radar system will not be dependent upon the computation time required to find these values.

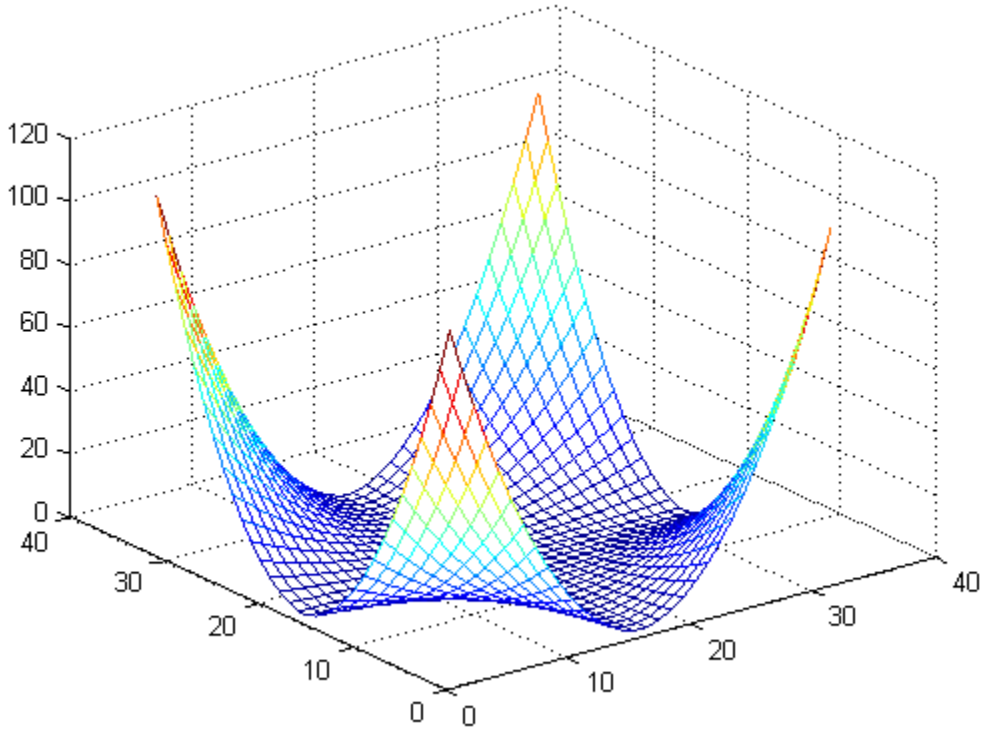

Figure 3.1: 2-Dimensional quadratic phase shift values

3.2 Calculation of Phase Shift Values

Before the theoretical equations developed in the previous section can be tested, phase shift values must be chosen to create the low gain basis patterns. As seen in Figure 2.2, the author of [22] chose a quadratic phase shift applied across the array. This served to defocus the beam and reduce the gain of the array. For the two-dimensional array, the quadratic pattern of the phase shift was reused, only transformed into a two dimensional pattern, as shown in Figure 3.1. First, one quarter of a two-dimensional quadratic was created with the equation

$$a = scale * (\frac{3}{N^2})^2 * (2\pi t)^2 \tag{3.12}$$

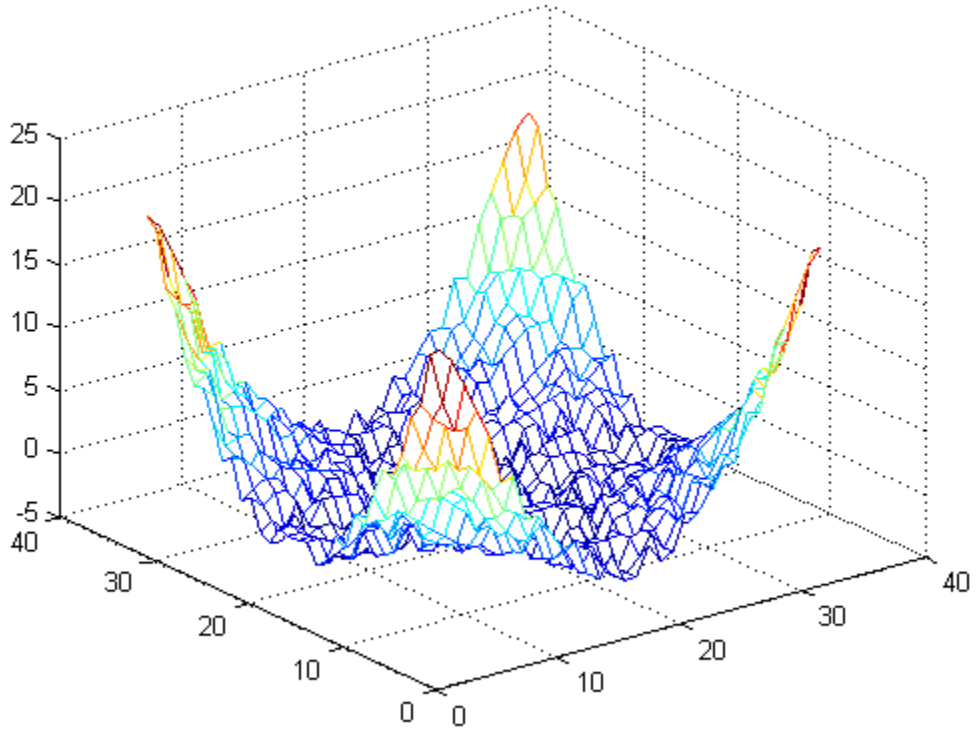

Figure 3.2: Alpha values used to create basis patterns for the two-dimensional array

which was then expanded to form the full quadratic. This pattern was then used to create an array pattern of the following form

$$f(\psi_n, \psi_m) = \sum_{n=0}^{N} \sum_{m=0}^{M} e^{j\alpha_{n,m}} e^{jn\psi_n} e^{jm\psi_m} \tag{3.13}$$

and the maximum gain of the pattern was calculated. A simulated annealing algorithm was then used to minimize this gain by manipulating the scalar scale of the equation. Once the optimal scale was found, the simulated annealing algorithm was again used to manipulate the individual α values in order to reduce the gain as much as possible. A tolerance of ± 1 for each point was used to reduce computation time. An example of the optimized phase shift values found is shown in Figure 3.2.

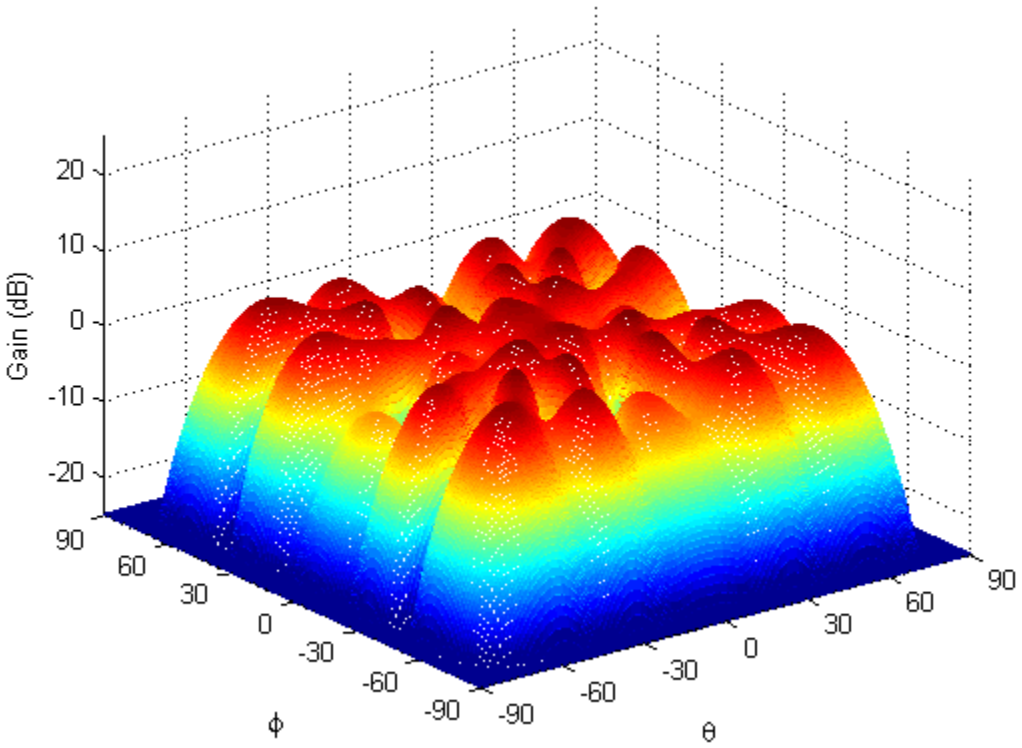

Figure 3.3: Fundamental basis pattern for an 8x8 array pattern

The resulting phase shift values created a low-gain, "spoiled" beam, as shown in Figure 3.3 for an 8x8 antenna array. The maximum gain of this spoiled pattern is approximately 4.7 dB, while the gain of the main lobe of the pattern without the applied phase shift is approximately 18 dB. Thus, it can be verified that by adding a certain series of phase shifts to an array pattern, such as the two-dimensional quadratic used above, the gain of the main beam of a pattern can be reduced significantly.

Chapter 4

Simulation Results

The MATLAB programming environment was used for all the following simulations, due to its advantages in handling the large matrix calculations needed in the discussed beamforming technique. As discussed in the development of the theory behind the technique, the bulk of the computational resources are needed only in calculating the complex coefficient weights used in the combination of the basis patterns. Once these coefficients are calculated, the weights can be applied to the returns of each individual basis function to form an equivalent high-gain beam.

4.1 Simulation Procedure

As discussed in Chapter 3, the field of view taken into consideration is defined by the range $-90^\circ \leq \theta \leq 90^\circ$ and $-90^\circ \leq \phi \leq 90^\circ$. The step size of θ and ϕ control the precision of the simulated far-field patterns. From the previous chapters, it is apparent that the calculation of the complex weights is not dependent upon θ and ϕ; therefore, the step size is only relevant for the simulation results. Because the ranges of θ and ϕ are constant, the values of $\psi_n = \beta d \sin(\theta)$ and $\psi_m = \beta d \sin(\phi)$ remain constant. Two arrays representing ψ_n and ψ_m were created and used throughout the simulations. For these simulations, the spacing between elements, d, in both the rows and the columns of the array was set to $\lambda/2$ so that $\psi_n = \pi \sin(\theta)$ and $\psi_m = \pi \sin(\phi)$. Because the arrays representing ψ_n and ψ_m remain constant throughout the development of the complex weights, the element spacing, as well as the frequency of the transmitted signal, can be changed without affecting the complexity of the computations.

The plots shown in the following sections are the general normalized power patterns of the array, expressed as [23]

$$P(\theta, \phi) = |F(\theta, \phi)|^2$$

where $F_i(\theta, \phi)$ has been defined in previous chapters as f_0, f_1, etc... This power pattern is further divided by the number of elements, N in the case of the one-dimensional array and N^2 in the case of the two-dimensional array, in order to normalize the patterns with regards to the number of elements in the array.

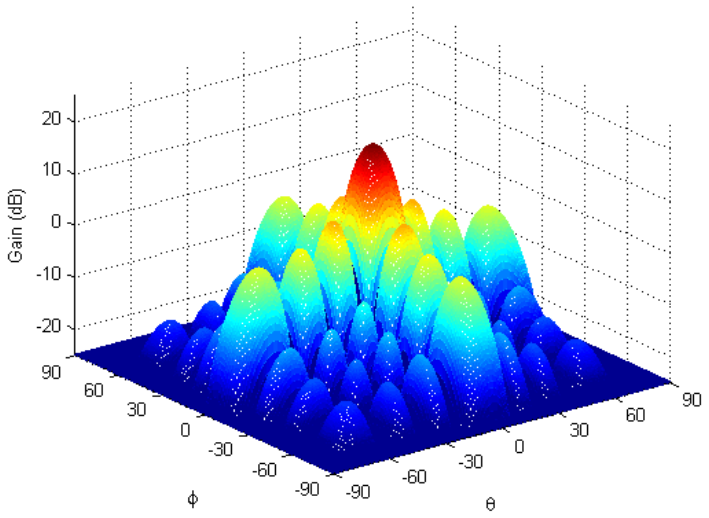

Figure 4.1: Fundamental array pattern for an 8x8 element array

4.2 Simulation Results for an 8x8 Element Array

The simulations were first run for an 8x8 element antenna array. As expected, the fundamental array pattern f_0, shown in Figure 4.1, demonstrates a high gain main lobe directed broadside to the array, as well as reduced sidelobes along the x and y axes. Figure 4.2 shows the pattern in the XZ plane, allowing clearer distinction of the main beam and side lobes. The fundamental basis pattern g_0 for the 8x8 array can be seen in Figure 4.3. As desired, this "spoiled" pattern exhibits lower, more uniform gain than the fundamental pattern. The peak gain of f_0 is approximately 18 dB, while the peak gain of g_0 is approximately 5 dB. This gain difference of 13 dB corresponds to an approximately 95% reduction in the intercept area.

Following the procedures developed in Chapter 3, a set of $8 * 8 = 64$ spoiled patterns were created, all possessing low, semi-uniform gain similar to Figure 4.3. Using these patterns, a set of complex coefficients were calculated to allow assembly of the scanned array patterns from a weighted summation of the 64 basis patterns. The recreated fundamental array, with the values $\theta = 0°$ and $\phi = 0°$, is shown in Figure 4.4.

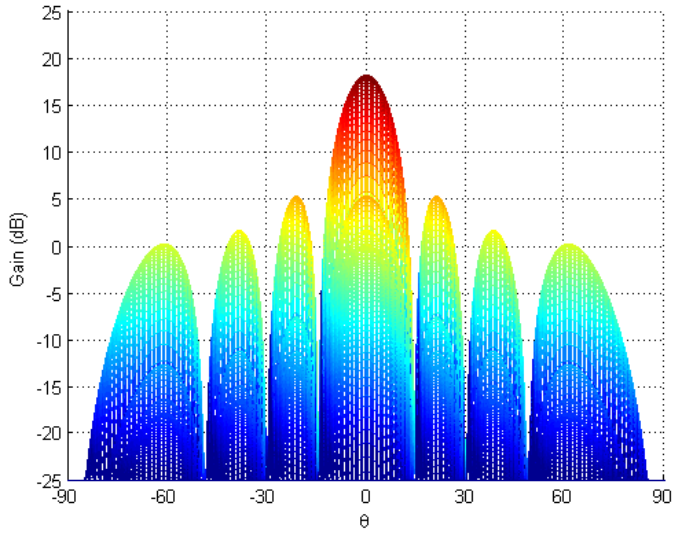

Figure 4.2: Fundamental array pattern for an 8x8 element array - XZ Plane

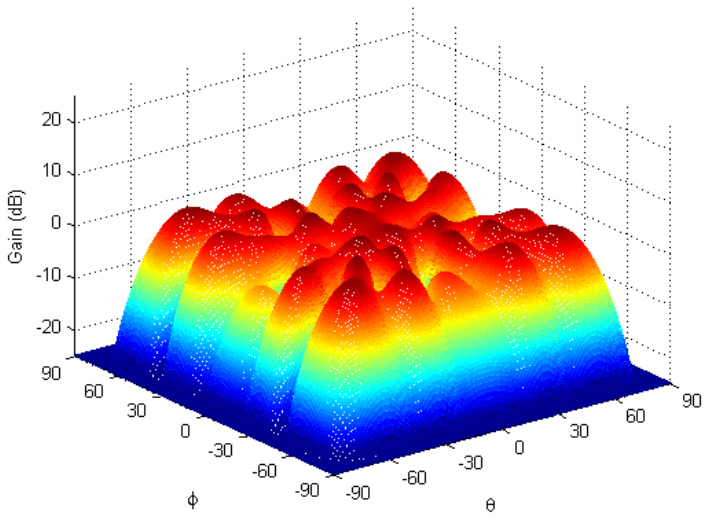

Figure 4.3: Fundamental basis pattern for an 8x8 element array - XZ Plane

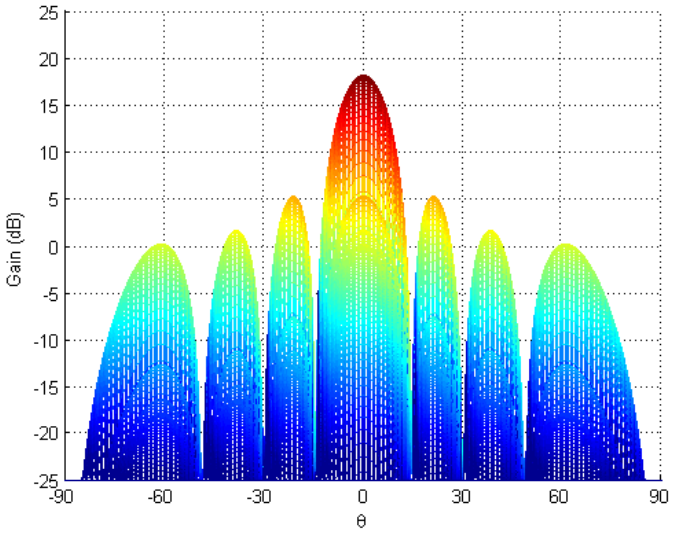

Figure 4.4: Recreated fundamental array pattern for an 8x8 element array

The recreated pattern appears to be virtually identical to the original fundamental pattern, and further analysis in MATLAB shows that the average difference between the two patterns is approximately 8×10^{-8} dB.

Similarly, each of the remaining 64 scanned array patterns can be recreated by the appropriate weighted summation of the basis patterns. After the complex coefficient values have been calculated, all of the scanned patterns can be constructed simultaneously. An example of one of the scanned patterns, with the main beam pointed at $\theta = -15°$ and $\phi = 15°$ can be seen in Figure 4.5. Each of the reconstructed patterns has the same beamwidth and gain of this pattern, the only difference being the pointing angle of the main beam.

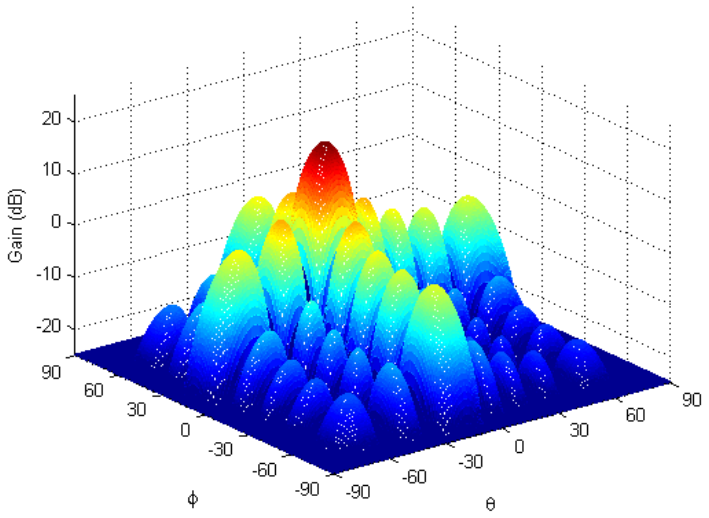

Figure 4.5: Recreated array pattern for an 8x8 element array with $\theta = -15°$ and $\phi = 15°$

4.3 Simulation Results for a 32x32 Element Array

Next, the simulations were run for a 32x32 element array. The fundamental array pattern of this array, when $\theta = 0°$ and $\phi = 0°$, is shown in Figures 4.6 and 4.7. Again, this pattern demonstrates a high gain main lobe directed broadside to the array and sidelobes along the x and y axes. As before, a set of $32 * 32 = 1024$ spoiled basis patterns were created. The fundamental basis pattern, when $\theta = 0°$ and $\phi = 0°$, is shown in Figure 4.8. The peak gain of the fundamental array pattern f_0 is approximately 30 dB, while the peak gain of the fundamental spoiled pattern is approximately 16 dB. This gain difference of 14 dB corresponds to an approximately 96% reduction in the intercept area.

Following the theory developed in Chapter 3, a set of complex coefficients were calculated to allow creation of the scanned array patterns from a weighted summation of these spoiled beams. The recreated fundamental array, once again with $\theta = 0°$ and $\phi = 0°$, is shown in Figure 4.9. Again, the recreated pattern appears to be virtually

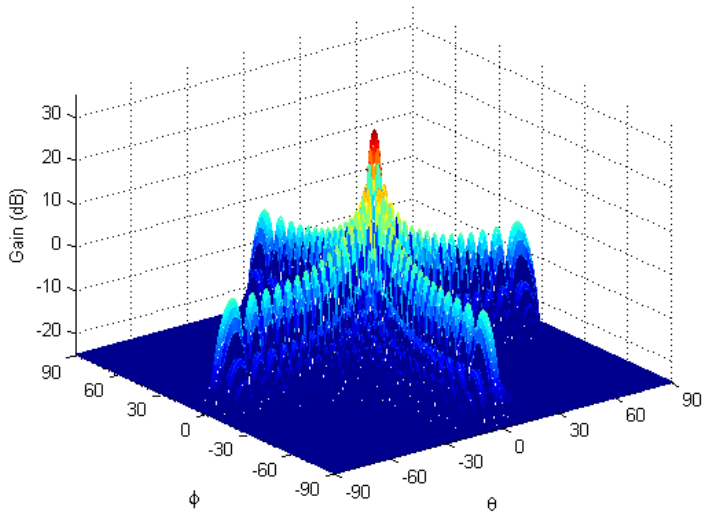

Figure 4.6: Fundamental array pattern for a 32x32 element array

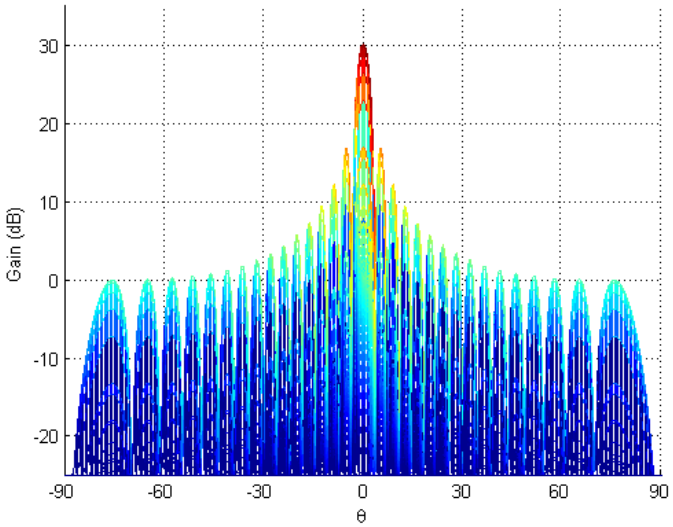

Figure 4.7: Fundamental array pattern for a 32x32 element array - XZ Plane

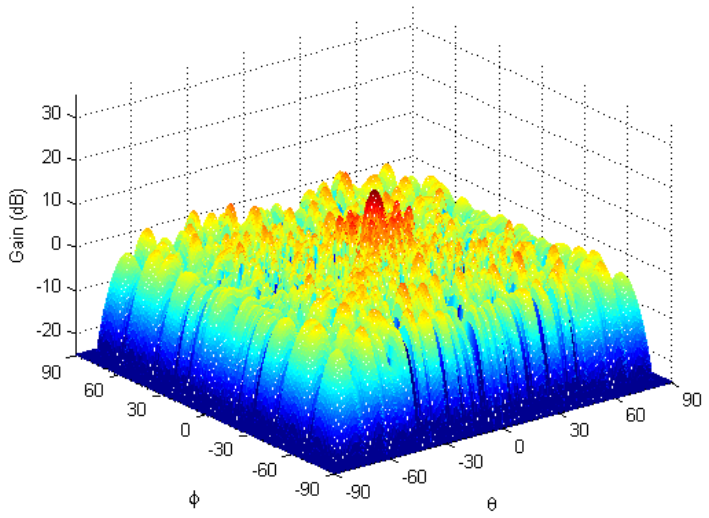

Figure 4.8: Fundamental basis pattern for a 32x32 element array

identical to the original fundamental pattern, with an average difference between the two patterns of approximately 5×10^{-15} dB. After the complex weights have been calculated, any scanned pattern can be recreated from the spoiled patterns. Figures 4.10, 4.11, and 4.12 show a recreated beam with scan angles of $\theta = 26°$ and $\phi = 44°$. As in the case of the 8x8 array in the previous section, all of the reconstructed patterns have the same bandwidth and gain as the original pattern.

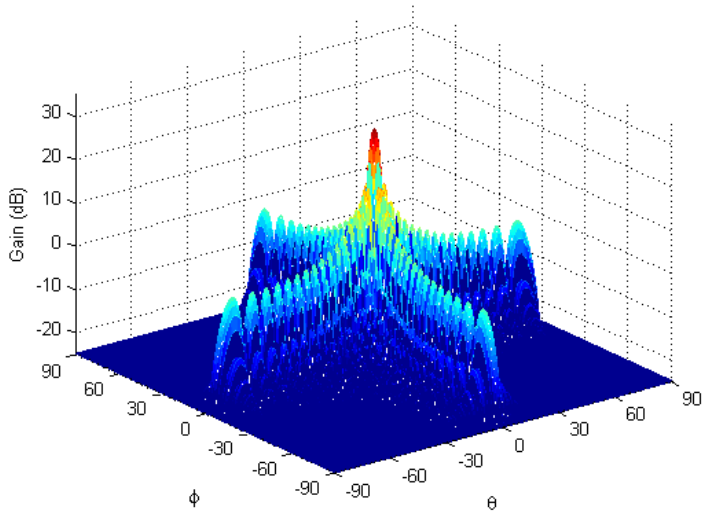

Figure 4.9: Recreated fundamental array pattern for a 32x32 element array

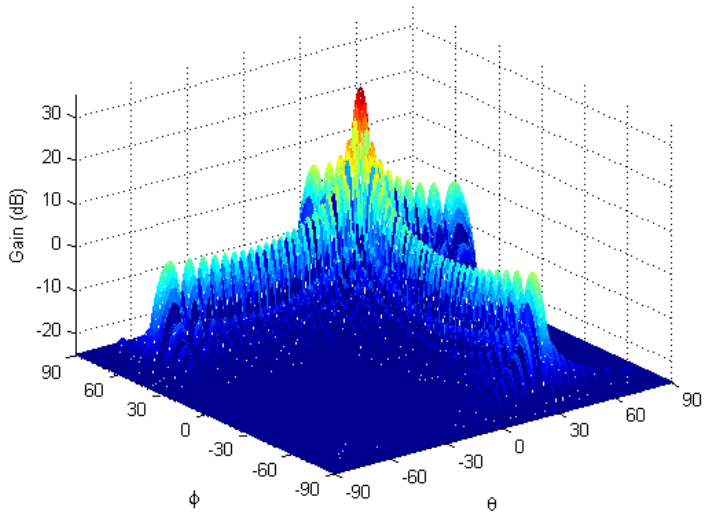

Figure 4.10: Recreated array pattern for a 32x32 element array with $\theta = 26°$ and $\phi = 44°$

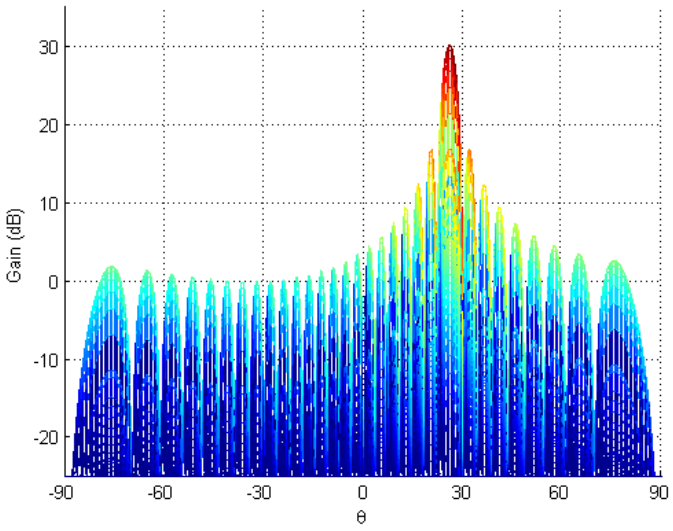

Figure 4.11: Recreated array pattern for a 32x32 element array with $\theta = 26°$ and $\phi = 44°$ - XZ Plane

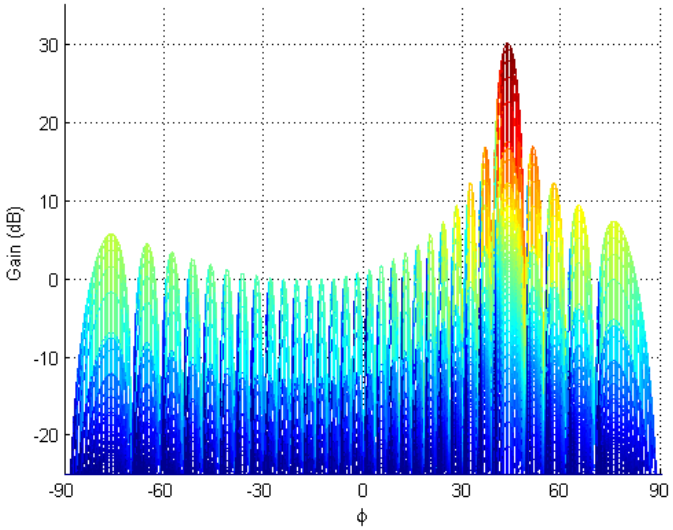

Figure 4.12: Recreated array pattern for a 32x32 element array with $\theta = 26°$ and $\phi = 44°$ - YZ Plane

Chapter 5

Implementation

5.1 Implementation Into an Existing Radar System

It has been shown that the high gain resulting from a traditional scanned main beam can be greatly reduced by using the method developed in Chapters 2 and 3. This technique involves replacing the high-gain beam resulting from a linear array with a weighted summation of a set of low gain, spoiled beams. In Chapter 4, it was shown that the beam patterns constructed from the superposition of these low gain basis patterns result in a far field pattern of similar shape and gain to that of the original high-gain pattern. As noted in the original development of the one-dimensional array in [22], this technique effectively trades transient peak power with sustained low power on the target over the search region, resulting in the same amount of total energy on the target.

In order to implement this theoretical approach into a practical radar system, the new beamforming technique must be integrated with the existing radar waveform. Many different waveforms can be used for different radar systems; however, the integration of this technique can most easily be observed with a standard pulsed waveform.

First, consider operation of a traditional waveform with a high-gain main lobe that is scanned across the search region. The beam is scanned by applying a linear phase progression across the elements of the array. If the phase-shifter settings of the system are designed so that the phase progression is increased with each pulse, then each pulse corresponds to a particular location of the scanned main beam. Likewise, if the phase shift values designed to form the low-gain patterns are applied across the

array, then each pulse corresponds to a particular low-gain basis pattern, i.e. pulse #1 for g_0, pulse #2 for g_1, etc... The returns of each pulse can then be processed through a matched filter and stored in memory. After all N pulses, and thus all N basis patterns, have been transmitted and received, the precalculated complex weights can be applied across the samples and summed. Each set of weights will result in the equivalent range return of a single high-gain main beam with the same phase progression. Once returns from all N basis patterns have been stored, any of the equivalent high-gain patterns can be formed simultaneously, requiring no additional scanning time when compared to the traditional method.

5.2 Two-way Analysis

In the theory developed in this paper, it is assumed that separate antenna arrays are used to transmit and receive, i.e., the pattern created from the antenna array is only affected on transmit. This is referred to as one-way synthesis. In developing the pattern theory for a one-dimensional array in [22], the author also considers the case where the same antenna array is used for both transmit and receive. In this scenario, the one-way pattern developed in Chapter 2 is not sufficient to fully describe the pattern seen by the receiver, as the target return must now be scaled by the square of the pattern. The synthesis of the resulting patterns is more complex than with separate antennas, and is accomplished by a linear combination of two-way basis patterns.

The analysis of the two-way pattern synthesis follows the same procedure as that for the one-way synthesis shown in Chapter 2; however, in each step the squared version of the patterns must be used. For example, for the case of the one-dimensional antenna array, instead of developing the expressions for $f_n(\psi)$ and $g_n(\psi)$, the analysis must now develop expressions for $f_n^2(\psi)$ and $g_n^2(\psi)$, respectively. Following this logic,

the weighted summation of the two-way basis patterns can now be written as

$$f_n^2(\psi) = \omega_{n,0} g_0^2(\psi) + \omega_{n,1} g_1^2(\psi) + \cdots + \omega_{n,2N-2} g_{2N-2}^2(\psi) \tag{5.1}$$

Because the squared versions of the patterns are used, $2N-1$ scanned patterns will be created, as opposed to the N scanned patterns created for one-way synthesis. It is shown in [22] that, in the context of the developed technique, two-way synthesis has comparable results to one-way synthesis. That is, each of the $2N-1$ scanned patterns can be recreated from a weighted summation of low gain spoiled patterns.

When considering the two-way synthesis for a two-dimensional antenna array, the complexity introduced by the squaring of the patterns increases the computational requirements greatly. When analyzing an array with NxN elements, one-way synthesis will result in N^2 basis patterns, requiring N^4 complex coefficients for the superposition of the spoiled patterns. Two way synthesis of this array would result in $2N^2-1$ basis patterns, requiring $2N^4-1$ complex coefficients. The mathematical complexity required to develop the matrix equations needed to solve for the complex coefficients is increased substantially. However, as in the case of one-way synthesis, all of these calculations can be completed prior to scanning. As a result, two-way synthesis would require no additional scanning time when compared to one-way synthesis, or to the traditional scanning method.

5.3 Computational Limitations

The computational complexity required to develop the needed set of spoiled basis functions and complex coefficients can vary greatly. With larger array sizes or smaller step sizes comes a greater required processing power. From the theoretical development shown in Chapter 3, it is evident that the creation of the set of spoiled patterns, as well as the calculation of the complex coefficients, is entirely dependent

upon the dimensions of the array and step size. Thus, all of the complex coefficient weights needed to accurately form an equivalent scanned pattern from the set of basis patterns can be calculated independently of the actual operation of the radar. This means that the radar itself is not responsible for any of the computationally intensive matrix calculations, but only for applying the previously calculated weights to the stored return information.

5.4 Hardware Requirements

As mentioned before, the low-gain basis patterns that need to be transmitted are simply the high-gain patterns of a traditional system spoiled by a certain phase shift. As a result, no additional hardware would have to be added to an existing array in order to transmit these beams; another phase scan would simply be added to each element before transmitting. The only other hardware needed to implement this technique would be a means of storing the returns of each of the N transmitted basis patterns, as well as the hardware necessary to carry out the weighted summation.

5.5 Doppler

It should be noted that, due to the importance of the phase relationship between basis patterns, a target must remain coherent over the scan time of the radar. If the target does not remain coherent, as would be likely in the case of long scan times, motion compensation may be required to allow for the target dynamics. This extra processing is a factor that must be considered when integrating this LPI technique with an existing radar system.

5.6 Areas for Future Research

There are several areas in which this research could be continued and expanded. First, it would be beneficial to work through the calculations to determine the matrix equations required to fully analyze the two-way synthesis pattern, as this is a scenario that is likely to occur in practical radar system. Second, it is possible that the gain of the basis beams could be reduced even further with continued research into finding the optimal phase shift values used to spoil the beams. Third, it would also be beneficial to explore integrating this method with the countless other waveforms used in radar systems for various objectives.

This paper has been focused primarily on the mathematics and theory of this technique. A great amount of research could be devoted to the integration of this method into the hardware of an existing radar system. Tests of actual radars implementing this technique need to be performed to verify the theory developed here.

Chapter 6

Conclusion

In [22], a method of improving the LPI performance of a linear antenna array was developed. This method involves replacing the high-gain main beam of a traditional scanning radar system with a set of low-gain, spoiled beams. These beams, which are simply the high-gain patterns spoiled by a certain phase shift, can be summed together to create returns equivalent to that of the traditional system. In this paper, the method was expanded from the case of a one-dimensional array to that of a two-dimensional array. This transition increases the complexity of the method, as the variations in the beam pattern must now be considered in both the x and y planes, or θ and ϕ, respectively.

After completing the required matrix calculations, simulations were run for both an 8x8 element array and a 32x32 element array. In the simulations of the 8x8 array, the peak gain of the main beam for the fundamental array pattern, when $\theta = 0^\circ$ and $\phi = 0^\circ$, was found to be approximately 18 dB. The peak gain of the fundamental basis pattern was found to be approximately 5 dB. This lower gain of the transmitted signal reduces the detection range of a hostile ESM system by a factor of $1/\sqrt{20}$, which corresponds to a 95% reduction in the intercept area of any potential hostile ESM systems.

In the simulations of the 32x32 element array, the peak gain of the main beam for the fundamental array pattern was found to be approximately 30 dB. The peak gain of the spoiled patterns was found to be approximately 16 dB. Again, this lower gain of the transmitted signal reduces the detection range of hostile ESM system by a factor of $1/\sqrt{25}$, corresponding to a 96% decrease in the intercept area.

In both of these cases, complex coefficients were calculated and and applied across the basis patterns. It was shown that a weighted summation of the complete set of spoiled patterns resulted in a return equivalent to that of the unspoiled pattern. When compared to the original fundamental pattern, the recreated pattern at $\theta = 0^\circ$ and $\phi = 0^\circ$ was found to differ by a negligible amount. The other weighted combinations of the basis patterns were also shown to provide returns equivalent to the high-gain patterns they replaced.

These results verify the claim made in [22]: that the high gain of single scanned main beam can be reduced by instead transmitting a set of spoiled beams, effectively replacing the transient high-power sweep with low power patterns radiated persistently while maintaining the same amount of energy on the target. The results for both the 8x8 and 32x32 element arrays show a significant decrease in intercept range, an advantage that could provide an existing system with obvious LPI performance increases. Although these improvements come at the cost of increased memory requirements and extra processing power, the technique has been shown to offer a promising method to reduce the visibility, and thus the probability of detection, of a radar attempting to avoid hostile ESM systems.

Bibliography

[1] Stephen L. Johnston, "Radar Electronic Counter-Countermeasures," *IEEE Transactions on Aerospace and Electronic Systems*, vol. AES-14, no. 1, pp. 109-117, Jan 1978.

[2] W. D. Wirth, "Long term coherent integration for a floodlight radar," in *Record of the IEEE 1995 International Radar Conference*, pp. 698-703, May 1995.

[3] F.A. Butt and M. Jalil, "An overview of electronic warfare in radar systems," in *2013 International Conference on Technological Advances in Electrical, Electronics and Computer Engineering (TAEECE)*, pp. 213-217, May 2013.

[4] Stephen L. Johnston, "CESM-a new category of radar ECCM," *IEEE Aerospace and Electronic Systems Magazine*, vol. 10, no. 2, pp. 36-38, Feb 1995.

[5] Mark A. Richards, James A. Scheer, and William A. Holm, "Principles of Modern Radar: Basic Principles," SciTech Publishing, 2010.

[6] A. G. Stove, A. L. Hume, and C. J. Baker, "Low probability of intercept radar strategies," *IEEE Proceedings - Radar Sonar and Navigation*, vol. 151, no. 5, pp. 249-260, Oct 2004.

[7] D. C. Schleher, "LPI radar: Fact or fiction," *IEEE Aerosp. Electron. Syst. Mag.*, vol. 21, pp. 3-6, May 2006.

[8] E. J. Carlson, "Low probability of intercept (LPI) techniques and implementations for radar systems," in *Proceedings of the 1988 IEEE NationalRadar Conference*, pp. 56-60, Apr 1988.

[9] F. B. Gross and K. Chen, "Comparison of detectability of traditional pulsed and spread spectrum radar waveforms in classic passive receivers," *IEEE Transactions on Aerospace and Electronic Systems*, vol. 41, no. 2, pp. 746-751, Apr 2005.

[10] P. Camuso, G. Foglia, and D. Pistoia, "A comprehensive analysis on detection performances of LPI signals filtering strategies," *European Radar Conference, 2009. EuRAD 2009*, pp. 125-128, Sep 30 2009 - Oct 2 2009.

[11] Y. D. Shirman, S. P. Leshchenko, and Y. M. Orlenko, "Advantages and problems of wideband radar," in *Proceedings of the International Radar Conference, 2003*, pp. 15-21, Sep 2003.

[12] K. L. Fuller, "To see and not be seen," in *IEE Proceedings F, Radar and Signal Processing* , vol. 137, no. 1, pp. 1-10, Feb 1990.

[13] A. G. Stove, "Linear FMCW radar techniques," in *IEE Proceedings F, Radar and Signal Processing*, vol. 139, no. 5, pp. 343-350, Oct 1992.

[14] Guo-Sui Liu, Hong Gu, Wei-min Su, and Hong-bo Sun, "The analysis and design of modern Low Probability of Intercept radar," in *Proceedings International Conference on Radar, 2001 CIE*, pp. 120-124, 2001.

[15] Guo-Sui Liu, Hong Gu, Wei-min Su, Hong-Bo Sun, and Jian-Hui Zhang, "Random signal radar - a winner in both the military and civilian operating environments," *IEEE Transactions on Aerospace and Electronic Systems*, vol. 39, no. 2, pp. 489-498, Apr 2003.

[16] M. A. Govoni, Hongbin Li, and J. A. Kosinski, "Low Probability of Interception of an Advanced Noise Radar Waveform with Linear-FM," *IEEE Transactions on Aerospace and Electronic Systems*, vol. 49, no. 2, pp. 1351-1356, Apr 2013.

[17] Sune R. J. Axelsson, "Noise radar using random phase and frequency modulation," *IEEE Transactions on Geoscience and Remote Sensing*, vol. 42, no. 11, pp. 2370-2384, Nov 2004.

[18] G. Schrick and R.G. Wiley, "Interception of LPI radar signals," in *Record of the IEEE 1990 International Radar Conference*, pp. 108-111, May 1990.

[19] J. Sanmartin-Jara, M. Burgos-Garcia, J. Cuesta-Acosta, and F. Perez-Martinez, "Tracking radar with LPI characteristics based on high rate SS-FH," *42nd Midwest Symposium on Circuits and Systems, 1999*, vol. 2, pp. 887-890, 1999.

[20] J. Vankka, "Digital frequency synthesizer/modulator for continuous-phase modulations with slow frequency hopping," *IEEE Transactions on Vehicular Technology*, vol. 46, no. 4, pp. 933-940, Nov 1997.

[21] Elie J. Baghdady, "Directional signal modulation by means of switched spaced antennas," *IEEE Transactions on Communications*, vol. 38, no. 4, pp. 399-403, Apr 1990.

[22] Dan Lawrence, "Low Probability of Intercept Antenna Array Beamforming," *IEEE Transactions on Antennas and Propagation*, vol. 58, no. 9, pp. 2858-2865, Sep 2010.

[23] Warren L. Stutzman and Gary A. Thiele, "Antenna Theory and Design," 2nd ed., John Wiley & sons, Inc., 1998.

Appendices

Appendix A

MATLAB Code

A.1 Optimize_phase_scan_2D.m

```
% Optimizes the phase shift values used to spoil
%  the array pattern

clear all
close all
clc

%% Optimize scale

MinimizeFunction = @minimizeGain_2D_scale;

scale = 0.5;

tic
[optimizedScale,gain1,exitFlag1,output] = ...
    simulannealbnd(MinimizeFunction, scale, 0, 1);
toc

%% Optimize individual values

MinimizeFunction = @minimizeGain_2D;

M = 32;
N = 32;
t = [N/2:-1:1]' * [N/2:-1:1];

x0 = optimizedScale * (3/N^2)^2 * (2*pi*t).^2;

for row = 1:length(x0)
    for col = 1:length(x0)
        lb(row,col) = x0(row,col) - 2;
        ub(row,col) = x0(row,col) + 2;
    end
end

[x,gain2,exitFlag2] = simulannealbnd(MinimizeFunction, x0, lb, ub);

alphas = x;
alphas = [alphas fliplr(alphas)];
alphas = [alphas; flipud(alphas)];
```

A.2 minimizeGain_2D_scale.m

```
% Minimizes gain of spoiled pattern by optimizing scale

function G = minimizeGain_2D_scale(scale)

M = 8;
N = 8;
t = [N/2:-1:1]' * [M/2:-1:1];

a = scale * (3/N^2)^2 * (2*pi*t).^2;

a = [a fliplr(a)];
a = [a; flipud(a)];

tN = 0:.1:pi;
tM = 0:.1:pi;
psiN = zeros(length(tN),length(tM));
psiM = zeros(length(tN),length(tM));

for timeIndexN = 1:length(tN)
    for timeIndexM = 1:length(tM)
        psiN(timeIndexN,timeIndexM) = pi*cos(tN(timeIndexN));
        psiM(timeIndexN,timeIndexM) = pi*cos(tM(timeIndexM));
    end
end

f = 0;
for indN = 1:N
    for indM = 1:M
        f = f + exp(1i*(a(indM,indN) + ((indN-1)*psiN + ...
            (indM-1)*psiM)));
    end
end

G = max(max(abs(f)))^2/(N^2);
```

A.3 minimizeGain_2D.m

```
% Minimizes gain of spoiled pattern by optimizing
%  individual alpha values

function G = minimizeGain_2D(a0)

a = [a0 fliplr(a0)];
a = [a; flipud(a)];

N = length(a);
M = N;

tN = 0:.1:pi;
tM = 0:.1:pi;

psiN = zeros(length(tN),length(tM));
psiM = zeros(length(tN),length(tM));

for timeIndexN = 1:length(tN)
    for timeIndexM = 1:length(tM)
        psiN(timeIndexN,timeIndexM) = pi*cos(tN(timeIndexN));
        psiM(timeIndexN,timeIndexM) = pi*cos(tM(timeIndexM));
    end
end

f = 0;
for indN = 1:N
    for indM = 1:M
        f = f + exp(1i*(a(indM,indN) + ((indN-1)*psiN + ...
            (indM-1)*psiM)));
    end
end

G = max(max(abs(f)))^2/(N^2);
```

A.4 Beamer_2D.m

```
clear all
close all
clc

%% Setup

load('8x8_alphas.mat','alphas');

N = size(alphas,1);
M = size(alphas,2);

tN = 0:.01:pi;
tM = 0:.01:pi;

r2d = 180 / pi;

%% Create plots of the fundamental patterns

psiN = zeros(length(tN),length(tM));
psiM = zeros(length(tN),length(tM));

for timeIndexN = 1:length(tN)
    for timeIndexM = 1:length(tM)
        psiN(timeIndexN,timeIndexM) = pi*cos(tN(timeIndexN));
        psiM(timeIndexN,timeIndexM) = pi*cos(tM(timeIndexM));
    end
end

f0 = 0;
g0 = 0;
for indN = 1:N
    for indM = 1:M
        f0 = f0 + exp(1i*((indN-1)*psiN + (indM-1)*psiM));
        g0 = g0 + exp(1i*(alphas(indN,indM) + (indN-1)*psiN + ...
            (indM-1)*psiM));
    end
end

f0_max = 10*log10(max(max(abs(f0)))^2/(N^2));
g0_max = 10*log10(max(max(abs(g0)))^2/(N^2));

g0_plot = 10*log10(abs(g0).^2/(N^2));
g0_plot(g0_plot <= -25) = -25;

f0_plot = 10*log10(abs(f0).^2/N^2);
f0_plot(f0_plot <= -25) = -25;

mesh(r2d*tN-90,r2d*tM-90,f0_plot);
axis([-90 90 -90 90 -25 35]);
zlabel('Gain (dB)'); xlabel('\theta'); ylabel('\phi');
```

```
set(gca,'Xtick',[-90 -60 -30 0 30 60 90],'Ytick',[-90 -60 -30 0 30 ...
    60 90])

figure
mesh(r2d*tN-90,r2d*tM-90,g0_plot);
axis([-90 90 -90 90 -25 35]);
zlabel('Gain (dB)'); xlabel('\theta'); ylabel('\phi');
set(gca,'Xtick',[-90 -60 -30 0 30 60 90],'Ytick',[-90 -60 -30 0 30 ...
    60 90])

%% Create all basis patterns

pscan = 2*pi/N;

g = cell(1,N^2);
for index = 1:N^2
    g{index} = zeros(size(psiN));
end

for a = 0:N-1
    for b = 0:M-1
        index = N*a + b + 1;
        for n = 0:N-1
            for m = 0:M-1
                g{index} = g{index} + exp(1i*(alphas(n+1,m+1) + ...
                    n*(psiN + a*pscan) + m*(psiM + b*pscan)));
            end
        end
    end
end

%% Calculate complex coefficent weights

A = zeros(N^2);
B = zeros(N^2);

for n = 0:N-1
    for m = 0:M-1
        row = N*n + m + 1;
        for a = 0:N-1
            for b = 0:M-1
                col = N*a + b + 1;
                A(row,col) = exp(1i*(alphas(n+1,m+1) + n*a*pscan + ...
                    m*b*pscan));
                B(row,col) = exp(1i*(n*a*pscan + m*b*pscan));
            end
        end
    end
end

coefficients = A\B;

%% Create f0

```

```
f0_new = zeros(size(psiN));
for index = 1:N^2
    f0_new = f0_new + coefficients(index,1)*g{index};
end

f0_new_max = 10*log10(max(max(abs(f0_new)))^2/(N^2));

difference = f0_new - f0;
ave_diff = mean(mean(abs(difference)));

f0new_plot = 10*log10(abs(f0).^2/N^2);
f0new_plot(f0new_plot <= -25) = -25;

figure
mesh(r2d*tN-90,r2d*tM-90,f0new_plot);
axis([-90 90 -90 90 -25 35]);
zlabel('Gain (dB)'); xlabel('\theta'); ylabel('\phi');
set(gca,'Xtick',[-90 -60 -30 0 30 60 90],'Ytick',[-90 -60 -30 0 30 ...
    60 90])

%% Create all fundamental array patterns

f = cell(1,N^2);
for index = 1:N^2
    f{index} = zeros(size(psiN));
end

for indexF = 1:N^2
    for indexG = 1:N^2
        f{indexF} = f{indexF} + coefficients(indexG,indexF)*g{indexG};
    end
end

for k=1:length(f)
    f_plot{k} = 10*log10(abs(f{k}).^2/N^2);
    f_plot{k}(f_plot{k} <= -25) = -25;
end

figure
mesh(r2d*tN-90,r2d*tM-90,f_plot);
axis([-90 90 -90 90 -25 35]);
zlabel('Gain (dB)'); xlabel('\theta'); ylabel('\phi');
set(gca,'Xtick',[-90 -60 -30 0 30 60 90],'Ytick',[-90 -60 -30 0 30 ...
    60 90])
```